MODELLING THE LIGHT FIELD IN MACROALGAE AQUACULTURE

A Thesis

Presented to

The Graduate Faculty of The University of Akron

In Partial Fulfillment

of the Requirements for the Degree

Master of Science

Oliver Graham Evans

May, 2018

MODELLING THE LIGHT FIELD IN MACROALGAE AQUACULTURE

Oliver Graham Evans

Thesis

Approved:	Accepted:
Advisor Dr. Kevin Kreider	Dean of the College Dr. John Green
Co-Advisor Dr. Curtis Clemons	Dean of the Graduate School Dr. Chand Midha
Department Chair Dr. Kevin Kreider	Date

ABSTRACT

A probabilistic model for the spatial distribution of kelp fronds is developed based on a kite-shaped geometry and simple assumptions about the motion of fronds due to water velocity. Radiative transfer theory is then applied to determine the radiation field by using the kelp model to determine optical properties of the medium. Finite difference and asymptotic solutions are explored, and behavior of the results over the parameter space is investigated. Flume experiments with synthetic kelp, combined with optical measurements of water and real kelp are used to determine model parameter values. Numerical simulations to predict the lifetime biomass production of kelp plants are performed to compare our light model to the previous exponential decay model. We find that everything works exactly as planned and everyone lives happily ever after.

Acknowledgments: This project was supported in part by the National Science Foundation under Grant No. EEC-1359256, and by the Norwegian National Research Council, Project number 254883/E40.

Mentors: Shane Rogers, Department of Environmental Engineering, Clarkson University; Ole Jacob Broch, and Aleksander Hand, SINTEF Fisheries and Aquaculture, Trondheim, Norway.

TABLE OF CONTENTS

LIST OF TABLES

Table Page

LIST OF FIGURES

CHAPTER I

INTRODUCTION

1.1 Motivation

Given the global rise in population, efficient and innovative resource utilization is increasingly important. In particular, food and fuel are clearly in high demand. Meanwhile, growing concern for the negative environmental impacts of petroleum-based fuel is generating a market for biofuel, especially corn-based ethanol. However, corn-based ethanol has been heavily criticized for diverting land usage away from food production. At the same time, a great deal of unutilized saltwater coastline is available for both food and fuel production through seaweed cultivation. Specifically, the sugar kelp *Saccharina Latissima* is known to be a viable source of food, both for direct human consumption and for fish cultivation, as well as for biofuel production. Industrial scale macroalgae cultivation has long existed in Eastern Asia due to the popularity of seaweed in Asian cuisine.

More recently, kelp aquaculture has been developing in Scandanavia and in the Northeastern United States. The MACROSEA project is a four year international research collaboration funded by the Research Council of Norway targeting "successful and predictable production of high quality biomass thereby making sig-

nificant steps towards industrial macroalgae cultivation in Norway." The project includes both cultivators and scientists, working to develop a precise understanding of the full lifecycle of kelp and its interaction with its environment. A fundamental aspect of this understanding is the development of mathematical models to describe the growth of kelp. Work is underway at SINTEF, a private Norwegian research institution, to develop such models. One aspect of the model which is has yet to be fully developed is the availability of light, considering factors such as absorption and scattering by the aquatic medium, as well as by the kelp itself.

In this thesis, the aquatic light field is investigated. As a first step, a model for the spatial distribution of kelp is developed. Radiative Transfer Theory is then applied to determine the effects of the kelp and water on the availability of light throughout the medium. We pursue a numerical finite difference solution to the Radiative Transfer Equation, and subsequently discuss asymptotic approximations which prove to be sufficiently accurate and less computationally intensive.

Frame as application: Dr. Rogers was approached by the operator of a wastewater treatment plant in Boothbay Harbor, Maine, who is facing increasingly demanding EPA regulations limiting the concentration of certain nutrients permissible to be released into the ocean via wastewater treatment outfalls. In order to adhere to these stricter requirements using conventional nutrient remediation, a significant quantity of specialized equipment would be necessary, which is not currently present in the Boothbay Harbor plant. Being surrounded on all sides by water and private property, the treatment plant lacks the necessary space for the additional

equipment, and would therefore need to move their entire facility to a new location in order to conform to these new nutrient regulations.

As an alternative to conventional nutrient remediation techniques, Dr. Rogers has proposed the cultivation of the macroalgae *Saccharina Latissima* (sugar kelp) near the outfall site. The purpose of such an undertaking would be twofold: to prevent eutrophication of the surrounding ecosystem by sequestering the nutrients in question, and to reduce one of the primary expenses in macroalgae cultivation: nutrient input. Once grown, a variety of products can be derived from macroalgae, including biofuel, fish/cattle feedstock, and high value chemical materials such as alginate and agar. Food for human consumption is also a common product of kelp aquaculture, though it may not be ideal for a wastewater treatment application.

Thus, we seek to investigate the feasibility, and optimal implementation of kelp farming in wastewater treatment operations. Specifically, I seek to develop an accurate model of the light field in a kelp farming environment as a function of both the spacing and depth of the kelp plants, and of the quality of the water itself. Ole Jacob Broch is a mathematician at SINTEF, a research organization in Trondheim, Norway, who has been working to model the growth of *Saccharina Latissima* using SINMOD, a large-scale 3D hydrodynamical ocean model developed at SINTEF. Ultimately, my aim is that my light model can be used both independently and in conjunction with Dr. Broch's SINMOD model.

1.2 Background on Kelp Models

Mathematical modeling of macroalgae growth is not a new topic, although it is a reemerging one. Several authors in the second half of the twentieth century were interested in describing the growth and composition of the macroalgae *Macrocystis pyrifera*, commonly known as "giant kelp," which grows prolifically off the coast of southern California. The very first such mathematical model was developed by W.J. North for the Kelp Habitat Improvement Project at the California Institute of Technology in 1968 using seven variables. By 1974, Nick Anderson greatly expanded on North's work, and created the first comprehensive model of kelp growth which he programmed using FORTRAN [1]. In his model, he accounts for solar radiation intensity as a function of time of year and time of day, and refraction on the surface of the water. He uses a simple model for shading, simply specifying a single parameter which determines the percentage of light which is allowed to pass through the kelp canopy floating on the surface of the water. He also accounts for attenuation due to turbidity using Beer's Law. Using this data on the availability of light, he calculates the photosynthesis rates and the growth experienced by the kelp.

Over a decade later in 1987, G.A. Jackson expanded on Anderson's model for *Macrocystis pyrifera*, with an emphasis on including more environmental parameters and a more complete description of the growth and decay of the kelp [2]. He takes into account respiration, frond decay, and most importantly for my work, sub-canopy light attenuation due to self-shading. He simply adds a coefficient to the exponen-

tial decay of light as a function of depth to represent shading from kelp fronds. He doesn't seem to consider and radial nor angular dependence on shading. Jackson also expands Anderson's definition of canopy shading, treating the canopy not as a single layer, but as 0, 1, or 2 discrete layers, each composed of individual fronds. While this is a significant improvement over Anderson's light model, it is still rather simplistic.

Both Anderson's and Jackson's model were carried out by numerically solving a system of differential equations over small time intervals. In 1990, M.A. Burgman and V.A. Gerard developed a stochastic population model [3]. This approach is quite different, and functions by dividing kelp plants into groups based on size and age, and generating random numbers to determine how the population distribution over these groups changes over time, based on measured rates of growth, death, decay, light availability, etc. That same year, Nyman et. al. tested a similar model in New Zealand, as well as a Markov chain model, and compared the results with experimental data [4].

In 1996 and 1998 respectively, P. Duarte and J.G. Ferreira used the size-class approach to create a more general model of macroalgae growth, and Yoshimori et. al. created a differential equation model of *Laminaria religiosa* with specific emphasis on temperature dependence of growth rate [5, 6]. These were the some of the first models of kelp growth that did not specifically relate to *Macrocystis pyrifera* ("giant

kelp"). Initially, there was a great deal of excitement about this species due to it's incredible size and growth rate, but difficulties in harvesting and negative environmental impacts have caused scientists to investigate other kelp species.

In the last five years, a team at SINTEF, a research organization associated with the Norwegian University of Technology and Science (NTNU), based in Trondheim, Norway, has become interested in the aquaculture potential of the kelp *Saccharina latissima* for use as food, animal feed, nutrient remediation, biofuel production, and high-value chemical production among other uses. In 2012, Ole Jacob Broch, whom I have been working with for the last few weeks, published a paper with Dag Slagstad describing the model they created of the growth and composition of *S. latissima* over the course of the year [7]. Their model works in conjunction with SINMOD, a 3D hydrodynamic ecosystem model developed at SINTEF which generates data on water temperature, water velocity, light intensity, and phytoplankton concentrations among other valuable quantities [8]. This detailed information has allowed Ole Jacob to consider many factors which influence the growth and decay of kelp in greater detail than has previously been explored.
*** Remove 1st person? ***

1.3 Background on Radiative Transfer

In terms of optical quantities, our primary interest is in the radiance at each point from all directions, which affects the photosynthetic rate of the kelp, and therefore

the total amount of biomass producible in a given area as well as the total nutrient absorption potential. The equation governing the radiance throughout the system is known as the Radiative Transfer Equation (RTE), which has been largely unutilized in the fields of oceanography and aquaculture. Meanwhile, it has been studied extensively in two fields: stellar astrophysics and computer graphics. In its full form, radiance is a function of 3 spatial dimensions, 2 angular dimensions, and frequency, making for an incredibly complex problem. Thus far, I have ignored the dependence on frequency, and have only considered monochromatic radiation. The RTE states that along a given path, radiance is decreased by absorption and scattering out of the path, while it is increased by emission and scattering into the path. In our situation, emission is negligible, owing only perhaps to some small luminescent phytoplankton or some such anomaly, and can therefore be safely ignored.

We use monochromatic radiative transfer in order to model the light field in an aqueous environment populated by vegetation. The vegetation (kelp) is modeled by a spatial probability distribution, which we assume to be given. The two quantities we seek to compute are *radiance* and *irradiance*. Radiance is the intensity of light in at a particular point in a particular direction, while irradiance is the total light intensity at a point in space, integrated over all angles. The Radiative Transfer Equation is an integro-partial differential equation for radiance, which has been used primarily in stellar astrophysics; it's application to marine biology is fairly recent [9].

Understanding the growth rate and nutrient recovery by kelp cultures has important marine biological implications. For example, recent work by our research

group at Clarkson University, the University of Maine, and SINTEF Fisheries and Aquaculture is investigating kelp aquaculture as a means to recover nutrients from wastewater effluent plumes in coastal environments into a valuable biomass feedstock for many products. Current models for kelp growth place little emphasis on the way in which nearby plants shade one another. Self-shading may be a significant model feature, though, as light availability may impact the growth and composition of the kelp biomass, and thus the mixture of goods that may be derived.

1.4 Summary of Main Results

CHAPTER II

MODEL DEVELOPMENT

2.1 Physical Setup

Being a salt water species, macroalgae cultivation occurs primarily in the ocean, with the exception of the initial stage of growth, where microscopic kelp spores are inoculated onto a thread in a small laboratory pool. This thread is then wrapped around a large rope, which is placed in the ocean and generally suspended by buoys in one of two configurations: horizontal or vertical. Thus far, I am primarily concerned with modeling the vertical rope case, in which the kelp plants extend radially outward from the rope in all directions, which are made up of a single frond (leaf), stipe (stem) and holdfast (root structure). We consider a rectangular grid of such vertical ropes. Plants extending from each rope will shade both themselves and their neighbors to varying degrees based on the depth of the kelp, the rope spacing, the angle of incident light on the surface and the nature of scattering in the water. In addition, light will be naturally absorbed by the water to varying degrees as determined by the clarity of the water.

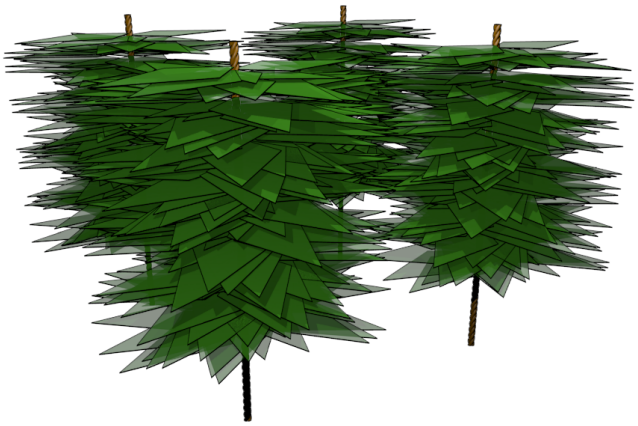

Figure 2.1: 4×4 array of vertical kelp ropes

2.1.1 Coordinate System

For all of our three dimensional analysis, we will use the absolute coordinate system defined in figure 2.2. In the following sections, we will wish to convert between Cartesian and spherical coordinates, which we will do using the following formulas.

$$\begin{aligned} x &= r \sin\phi \cos\theta \\ y &= r \sin\phi \sin\theta \\ z &= r \cos\phi \end{aligned} \tag{2.1}$$

Therefore, for some function $f(x, y, z)$, we can write its derivative along a path in spherical coordinates in terms of Cartesian coordinates using the chain rule.

$$\frac{\partial f}{\partial r} = \frac{\partial f}{\partial x}\frac{\partial x}{\partial r} + \frac{\partial f}{\partial y}\frac{\partial y}{\partial r} + \frac{\partial f}{\partial z}\frac{\partial z}{\partial r} \tag{2.2}$$

Then, calculating derivatives from (2.1), we get

$$\frac{\partial f}{\partial r} = \frac{\partial f}{\partial x}\sin\phi\cos\theta + \frac{\partial f}{\partial y}\sin\phi\sin\theta + \frac{\partial f}{\partial z}\cos\phi \tag{2.3}$$

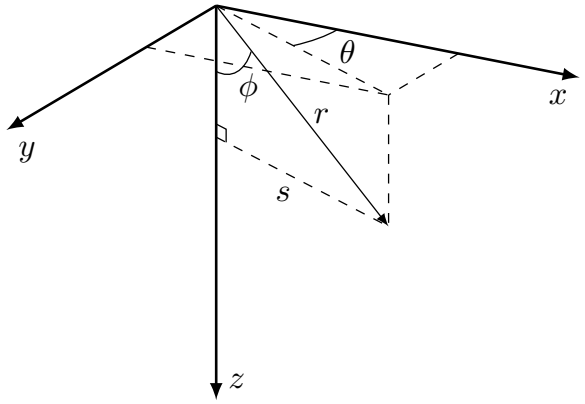

Figure 2.2: Downward-facing right-handed coordinate system with radial distance r from the origin, distance s from the z axis, zenith angle ϕ and azimuthal angle θ

2.1.2 Domain

Let the domain be defined as

$$\begin{aligned} D = \big\{\vec{x} \in \mathbb{R}^3 : & x_{\min} \le \vec{x}\cdot\hat{x} \le x_{\max} \\ & \text{and } y_{\min} \le \vec{x}\cdot\hat{y} \le y_{\max} \\ & \text{and } z_{\min} \le \vec{x}\cdot\hat{z} \le z_{\max}\big\} \end{aligned} \tag{2.4}$$

Let the surface and bottom of the domain be denoted respectively by

$$S = \{\vec{x_s} \in D : \vec{x_s}\cdot\hat{z} = 0\} \tag{2.5}$$

$$B = \{\vec{x_b} \in D : \vec{x_b}\cdot\hat{z} = 0\} \tag{2.6}$$

2.2 Kelp Model

2.2.1 Frond shape

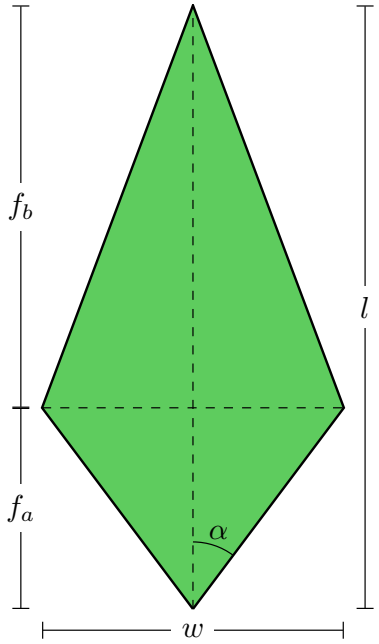

Figure 2.3: Model frond diagram

We assume the frond is a kite with length l from base to tip, and width w from left to right. The shortest distance from the base to the diagonal connecting the left and right corners is called f_a, and the shortest distance from that diagonal to the tip is called f_b. We have

$$f_a + f_b = l \tag{2.7}$$

When considering a whole population with varying sizes, it is more convent to specify

ratios than absolute lengths. Let the following ratios be defined.

$$f_r = \frac{l}{w} \tag{2.8}$$

$$f_s = \frac{f_a}{f_b} \tag{2.9}$$

These ratios are assumed to be consistent among the entire population, making all fronds geometrically similar. With these definitions, the shape of the frond can be fully specified by l, f_r, and f_s. It is possible, then, to redefine w, f_a and f_b as follows from the preceding formulas.

$$w = \frac{l}{f_r} \tag{2.10}$$

$$f_a = \frac{l f_s}{1 + f_s} \tag{2.11}$$

$$f_b = \frac{l}{1 + f_s} \tag{2.12}$$

The angle α, half of the angle at the base corner, will be important in our analysis. Using the above equations,

$$\alpha = \tan^{-1}\left(\frac{2 f_r f_s}{1 + f_s}\right) \tag{2.13}$$

2.2.2 Length distribution

*** Normal Distribution ***

2.2.3 Frond angle distribution

We assume the frond angle varies according to the von Mises distribution, which is the periodic analogue of the normal distribution. It is defined on $[-\pi, \pi]$ rather than

$(-\infty, \infty)$. It has two parameters, μ and κ, which shift and sharpen the distribution respectively. κ can be considered analogous to $1/\sigma$ in the normal distribution. Here, we use $\mu = \theta_w$ and $\kappa = v_w$.

The PDF for this distribution is

$$P_{\theta_f}(\theta_f) = \frac{\exp\left(v_w \cos(\theta_f - v_w)\right)}{2\pi I_0(v_w)} \tag{2.14}$$

where $I_0(x)$ is the modified Bessel function of the first kind of order 0. Notice that unlike the normal distribution, the von Mises distribution approaches a *non-zero* uniform distribution as κ approaches 0.

$$\lim_{v_w \to 0} P_{\theta_f}(\theta_f) = \frac{1}{2\pi} \; \forall \, \theta_f \in [-\pi, \pi] \tag{2.15}$$

The idea behind using this distribution is that with zero current velocity, the frond angles should be distributed uniformly, while as current velocity increases, they should be increasingly likely to be pointing in the direction of the current. Note that θ_w and v_w are functions of position. For a given depth layer, we will use the average water velocity for that depth.

2.2.4 Combined 2D length-angle distribution

The previous two distributions can reasonably be assumed to be independent of one another. That is, the angle of the frond does not depend on the length, or vice versa. Therefore, the probability of a frond simultaneously having a given frond length and angle is the product of their individual probabilities.

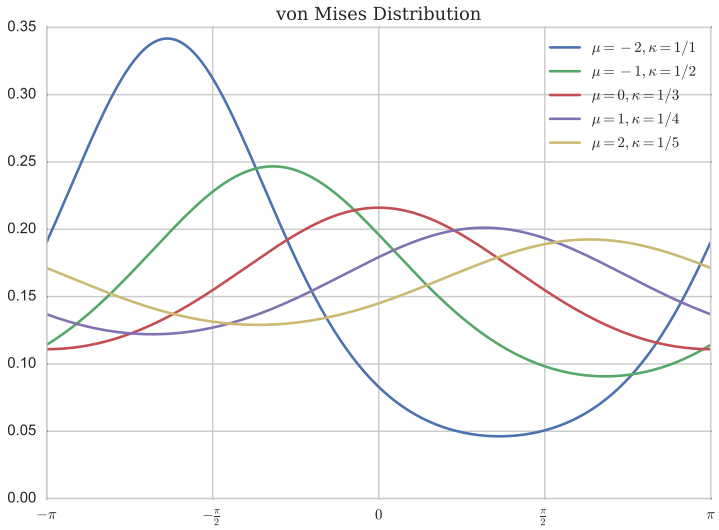

Figure 2.4: von Mises distribution for a variety of parameters

Given independent events A and B,

$$P(A \cap B) = P(A)P(B) \tag{2.16}$$

Then the probability of frond length l and frond angle θ_f coinciding is

$$P_{2D}(\theta_f, l) = P_{\theta_f}(\theta_f) \cdot L(l) \tag{2.17}$$

A contour plot of this 2D distribution for a specific set of parameters is shown in figure 2.5, where probability is represented by color in the 2D plane. Darker green represents higher probability, while lighter beige represents lower probability. In figure 2.6, 50 samples are drawn from this distribution and plotted.

It is important to note that if P_{θ_f} were dependent on l, the above definition of P_{2D} would no longer be valid. For example, it might be more realistic to say that

larger fronds are less likely to bend towards the direction of the current. In this case, (2.16) would no longer hold, and it would be necessary to use the following more general relation.

$$P(A \cap B) = P(A)P(B|A) = P(B)P(B|A) \tag{2.18}$$

This is currently not taken into consideration in this model.

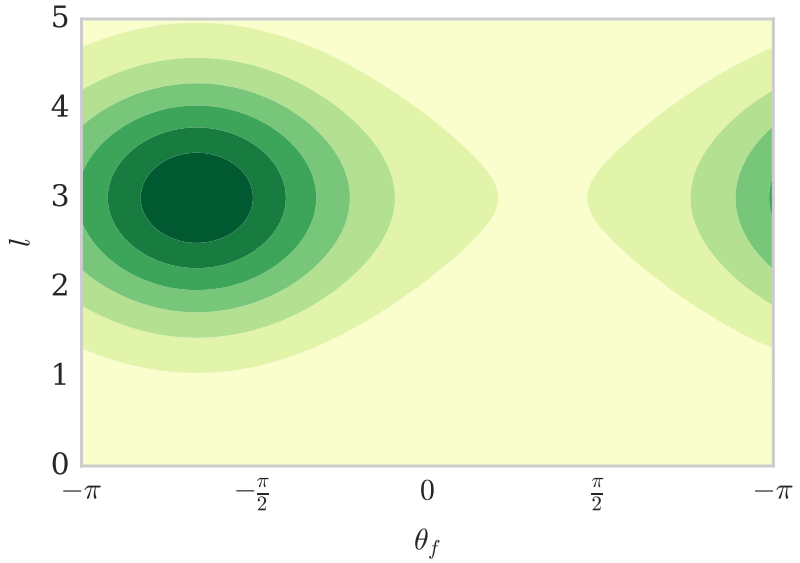

Figure 2.5: 2D length-angle probability distribution with $\theta_w = 2\pi/3, v_w = 1$

2.3 Light Model

2.3.1 Optical Definitions

One of the most fundamental quantities in optics is radiant flux Φ, which is the has units of energy per time. The quantity of primary interest in modeling the light field is radiance L, which is defined as the radiant flux per steradian per projected surface

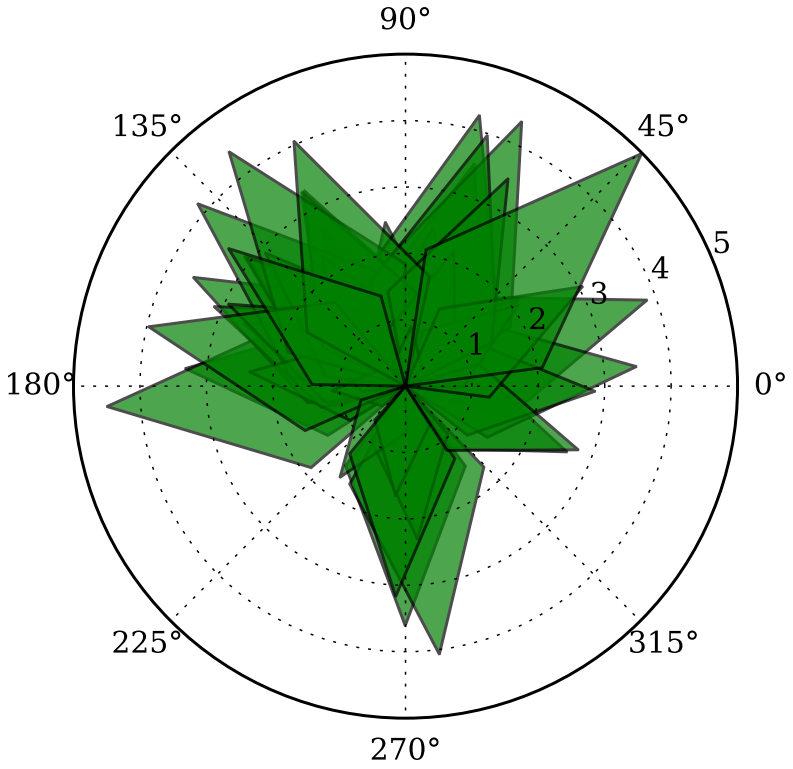

Figure 2.6: A sample of 50 kelp fronds with length and angle picked from the distribution above with $f_s = 0.5$ and $f_r = 2$.

area perpendicular to the direction of propagation of the beam. That is,

$$L = \frac{d^2\Phi}{dAd\omega} \tag{2.19}$$

We must now define a few inherent optical properties (IOPs) which depend only on the medium of propagation.

Consider a beam of light traveling through the water in the direction $\underline{\omega} = (\theta, \phi)$. As it travels, there will be some decrease in the radiance due to scattering and absorption. Let a_w and b_w be the coefficients of absorption and scattering respectively

due solely to the water. Similarly, define a_k and b_k to be the absorption and scattering coefficients due solely to kelp. The loss due to scattering or absorption, whether by kelp or water, is proportional to radiance, and a_w, b_w, a_k, b_k all have units of inverse meters.

There will also be some gain into the path of the beam due to scattering from other directions, as determined by the *volume scattering function*, $\beta(\Delta\theta) : [0, \pi) \to \mathbb{R}^+$, which gives the proportion of incident radiance scattered at an angle $\Delta\theta$ from its original direction due to only water. The units of β are $\mathrm{m}^{-1}\mathrm{sr}^{-1}$.

For convenience, let $\beta(\underline{\omega}_1, \underline{\omega}_2) = \beta\left(\cos^{-1}\left(\frac{\underline{\omega}_1 \cdot \underline{\omega}_2}{||\underline{\omega}_1||||\underline{\omega}_1||}\right)\right)$.

2.3.2 RTE: 1D

Consider a fixed position $\vec{x}$ and direction $\vec{\omega}$ such that $\vec{\omega} \cdot \hat{z} \neq 0$.

** Just call $\vec{x_0}$ a point, not a function. Call it the projection to the surface.

Let $\vec{l}(\vec{x}, \vec{\omega}, s)$ denote the linear path containing $\vec{x}$ with initial z coordinate given by

$$z_0 = \begin{cases} 0, & \vec{\omega} \cdot \hat{z} < 0 \\ z\mathrm{max}, & \vec{\omega} \cdot \hat{z} > 0 \end{cases} \tag{2.20}$$

Then,

$$\vec{l}(\vec{x}, \vec{\omega}, s) = \frac{1}{\tilde{s}}(s\vec{x} + (\tilde{s} - s)\vec{x_0}(\vec{x}, \vec{\omega})) \tag{2.21}$$

where

$$\vec{x_0}(\vec{x}, \vec{\omega}) = \vec{x} - \tilde{s}\vec{\omega} \tag{2.22}$$

is the origin of the ray, and

$$\tilde{s} = \frac{\vec{x} \cdot \hat{z} - z_0}{\vec{\omega} \cdot \hat{z}} \tag{2.23}$$

is the path length from $\vec{x_0}(\vec{x}, \vec{\omega})$ to $\vec{x}$.

2.3.3 Colloquial Description

Denote the radiance at $\vec{x}$ in the direction $\vec{\omega}$ by $L(\vec{x}, \vec{\omega})$. As light travels along $\vec{l}(\vec{x}, \vec{\omega}, s)$, interaction with the medium produces three phenomena of interest:

1. Radiance is decreased due to absorption.

2. Radiance is decreased due to scattering out of the path to other directions.

3. Radiance is increased due to scattering into the path from other directions.

2.3.4 IOPs

These phenomena are governed by three inherent optical properties (IOPs) of the medium. The absorption coefficient $a(\vec{x})$ (units m^{-1}) defines the proportional loss of radiance per unit length. The scattering coefficient b (units m^{-1}), defines the proportional loss of radiance per unit length, and is assumed to be constant over space.

The volume scattering function (VSF) $\beta(\Delta) : [0, \pi] \to \mathbb{R}^+$ (units sr^{-1}) defines the proportion of radiance scattered at an angle Δ from it's original direction. The VSF is normalized such that $\int_0^\pi \beta(\Delta)\, d\Delta = 1$. The scattering coefficient b can be considered the magnitude of the unnormalized VSF.

2.3.5 Equation of Transfer

Then, combining these phenomena, the Radiative Transfer equation along $\vec{l}(\vec{x},\vec{\omega})$ becomes

$$\frac{dL}{ds}(\vec{l}(\vec{x},\vec{\omega},s),\vec{\omega}) = -(a(\vec{x})+b)L(\vec{x},\vec{\omega}) + b\int_{4\pi}\beta(|\vec{\omega}-\vec{\omega}'|)L(\vec{x})\,d\omega', \tag{2.24}$$

where $\int_{4\pi}$ denotes integration over the unit sphere and $|\vec{\omega}-\vec{\omega}'| = \cos^{-1}(|\vec{\omega}-\vec{\omega}'|)$.

2.3.6 RTE: Vector

Now, we have

$$\begin{aligned}\frac{dL}{ds}(\vec{l}(\vec{x},\vec{\omega},s),\vec{\omega}) &= \frac{d\vec{l}}{ds}(\vec{x},\vec{\omega},s)\cdot\nabla L(x,\vec{\vec{\omega}},\vec{\omega}) \\ &= \vec{\omega}\cdot\nabla L(\vec{x},\vec{\omega})\end{aligned}$$

Then, the general form of the Radiative Transfer Equation is

$$\vec{\omega}\cdot\nabla L(\vec{x},\vec{\omega}) = -(a(\vec{x})+b)L(\vec{x},\vec{\omega}) + b\int_{4\pi}\beta(|\vec{\omega}-\vec{\omega}'|)L(\vec{x},\vec{\omega}')\,d\omega' \tag{2.25}$$

or, equivalently,

$$\vec{\omega}\cdot\nabla L(\vec{x},\vec{\omega}) + a(\vec{x})L(\vec{x},\vec{\omega}) = b\left(\int_{4\pi}\beta(|\vec{\omega}-\vec{\omega}'|)L(\vec{x},\vec{\omega}')\,d\omega' - L(\vec{x},\vec{\omega})\right) \tag{2.26}$$

2.3.7 Boundary Conditions

We use periodic boundary conditions in the x and y directions.

$$L\left((x_{\min},y,z),\vec{\omega}\right) = L\left((x_{\max},y,z),\vec{\omega}\right) \tag{2.27}$$

$$L\left((x,y_{\min},z),\vec{\omega}\right) = L\left((x,y_{\max},z),\vec{\omega}\right) \tag{2.28}$$

In the z direction, we specify a spatially uniform downwelling light just under the surface of the water by a function $f(\vec{\omega})$.

* $z_{\min}$ could also be much lower, e.g. 5m.

Further, we assume that no upwelling light enters the domain from the bottom.

$$L(\vec{x_s}, \vec{\omega}) = f(\omega) \text{ if } \vec{\omega} \cdot \hat{z} > 0 \tag{2.29}$$

$$L(\vec{x_b}, \vec{\omega}) = 0 \text{ if } \vec{\omega} \cdot \hat{z} < 0 \tag{2.30}$$

2.3.8 Radiative Transfer

Let n be the number of spatial dimensions for the problem (i.e., 2 or 3). Let $x \in \mathbb{R}^n$. Let Ω be the unit sphere in $\mathbb{R}^n$. Let $\omega \in \Omega$ be a unit vector in $\mathbb{R}^n$. Let $L(x, \omega)$ denote *radiance* position x in the direction ω. Let $I(x)$ denote *irradiance* at position x. Let $P_k(x)$ be the probability density of kelp at position x. Let a_w and a_k be the absorption coefficients of water and kelp respectively. Let b_w and b_k be the scattering coefficients of water and kelp respectively. Then we define the effective absorption and scattering coefficients as

$$a(x) = P_k(x)a_k + (1 - P_k(x))a_w \tag{2.31}$$

$$b(x) = P_k(x)b_k + (1 - P_k(x))b_w \tag{2.32}$$

Then, the Monochromatic Time-Independent Radiative Transfer Equation (RTE) is

$$\begin{aligned} \omega \cdot \nabla_x L(x, \omega) = &-(a(x) + b(x))L(x, \omega) \\ &+ b \int_\Omega \beta(\omega \cdot \omega') L(x, \omega')\, d\omega' \end{aligned} \tag{RTE}$$

Note that in 2 spatial dimensions, this is a 3-dimensional problem (x, y, θ). Likewise, in 3 spatial dimensions, it is a 5-dimensional problem (x, y, z, θ, ϕ).

In this paper, we consider only the 2-dimensional problem, with the hope that sufficiently robust solution techniques for the 2-dimensional problem will be effective in the solution of the 3-dimensional problem as well.

2.3.9 Boundary Conditions

We assume that the downwelling light from the surface is known, and is defined to be uniform in space by the Dirichlet boundary condition

$$L(x, 0, \theta) = f(\theta), \quad \text{for} \quad \theta \in [0, \pi). \tag{2.33}$$

Note that we cannot apply the same idea to upwelling light at the surface, as it cannot be specified from information about the atmospheric light field. Therefore, we apply the PDE at $y = 0$ for $\theta \in [\pi, 2\pi)$.

At $y = 1$, we assume no upwelling light. That is,

$$L(x, 0, \theta) = 0, \quad \text{for} \quad \theta \in [\pi, 2\pi). \tag{2.34}$$

As with the upper y-boundary, we apply the PDE for $\theta \in [0, \pi)$ so as not to prohibit downwelling light.

In the horizontal direction, we assume periodic boundary conditions. Assuming that a single discrete group of plants is being simulated, adjusting the width of the domain effectively modifies the spacing between adjacent groups of plants.

CHAPTER III

SOLUTION PROCEDURE

3.1 Calculate Kelp Density

3.1.1 Relative coordinate system

To determine under what conditions a frond will shade a given point, we begin by describing the shape of the frond in Cartesian and then converting to polar coordinates. Of primary interest are the edges connected to the frond tip. For convenience, we will use a relative coordinate system (θ', s) such that the line connecting the base to the tip is vertical, with the base at $(0, 0)$. The Cartesian analogue of this coordinate system, (x', y'), has the following properties.

$$x' = s\cos\theta' \tag{3.1}$$

$$y' = s\sin\theta' \tag{3.2}$$

and

$$s = \sqrt{x'^2 + y'^2} \tag{3.3}$$

$$\theta' = \text{atan2}(y, x) \tag{3.4}$$

3.1.2 Functional description of frond edge

With this coordinate system established, we can describe the outer two edges of the frond in Cartesian coordinates as a piecewise linear function connecting the left corner: $(-w/2, f_a)$, the tip: $(0, l)$, and the right corner: $(w/2, f_a)$. This function has the form

$$y'_f(x') = l - \text{sign}(x')\frac{f_b}{w/2}x'. \tag{3.5}$$

Using the equations in section 3.1.1, this can be written in polar coordinates after some rearrangement as

$$s'_f(\theta') = \frac{l}{\sin\theta' + S(\theta')\frac{2f_b}{w}\cos\theta'} \tag{3.6}$$

where

$$S(\theta') = \text{sign}(\theta' - \pi/2) \tag{3.7}$$

Then, using the relationships in section 2.2.1, we can rewrite the above equation in terms of our frond ratios f_s and f_r.

$$s'_f(\theta') = \frac{l}{\sin\theta' + S(\theta')\frac{2f_r}{1+f_s}\cos\theta'} \tag{3.8}$$

3.1.3 Absolute coordinates

To generalize to a frond pointed at an angle θ_f, we will use the coordinate system (θ, s) such that

$$\theta = \theta' + \theta_f - \frac{\pi}{2} \tag{3.9}$$

Then, for a frond pointed at the arbitrary angle θ_f, the function for the outer edges can be written as

$$s_f(\theta) = s'_f\left(\theta - \theta_f + \frac{\pi}{2}\right) \tag{3.10}$$

3.1.4 Conditions for occupancy

Consider a fixed frond of length l at an angle θ_f. The point (θ, s) is occupied by the frond if

$$|\theta_f - \theta| < \alpha \tag{3.11}$$

and

$$s < s_f(\theta) \tag{3.12}$$

Equivalently, letting the point (θ, s) be fixed, a frond occupies the point if the following conditions are satisfied.

$$\theta - \alpha < \theta_f < \theta + \alpha \tag{3.13}$$

and

$$l > l_{min}(\theta, s) \tag{3.14}$$

where

$$l_{min}(\theta, s) = s \cdot \frac{l}{s_f(\theta)} \tag{3.15}$$

Then, considering the point to be fixed, (3.13) and (3.14) define the spacial region $R_s(\theta, s)$ called the "occupancy region for (θ, s)" with the property that if the tip of a frond lies within this region (i.e. $(\theta_f, l) \in R_s(\theta, s)$), then it occupies

the point. $R_s(3\pi/4, 3/2)$ is shown in blue in figure 3.1 and the smallest possible occupying fronds for several values of θ_f are shown in various colors. Any frond longer than these at the same angle will also occupy the point.

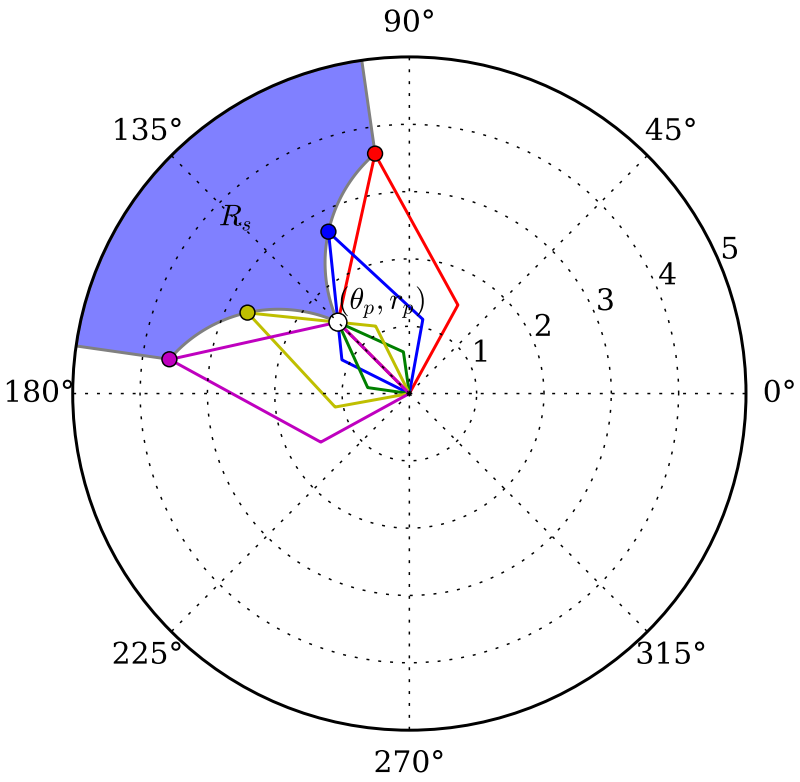

Figure 3.1: Outlines of minimum-length fronds for a variety of angles to occupy the point $(\theta, s) = (3\pi/4, 3/2)$

3.1.5 Probability of occupancy

NOT SO SURE ABOUT THIS

Now, we are able to define the probability of a frond occupying the point

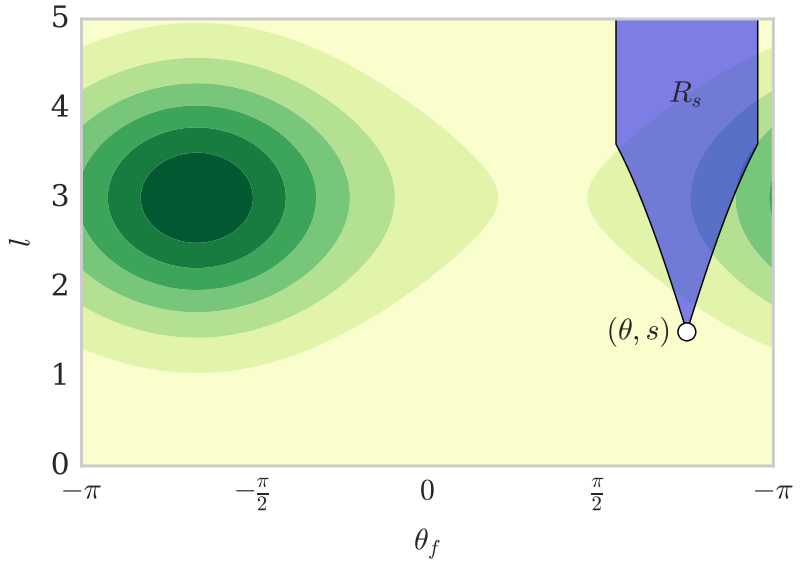

Figure 3.2: Contour plot of $P_{2D}(\theta_f, l)$ overlayed with the region in the $\theta_f - l$ plane which results in a frond occupying the point $(\theta, s) = (3\pi/4, 3/2)$

(θ, s) at a depth z at time t by

$$\begin{aligned} P_k(\theta, s, z, t) &= \iint_{R_s(\theta,s,z,t)} P_{2D}(\theta_f, l)\ dl\ d\theta_f \\ &= \int_{\theta-\alpha}^{\theta+\alpha} \int_{l_{min}(\theta_f,z,t)}^{\infty} P_{2D}(\theta_f, l)\ dl\ d\theta_f \end{aligned} \tag{3.16}$$

3.2 Asymptotics

3.2.1 Substitute asymptotic series

$$L(\vec{x}, \vec{\omega}) = L_0(\vec{x}, \vec{\omega}) + bL_1(\vec{x}, \vec{\omega}) + b^2 L_2(\vec{x}, \vec{\omega}) + \cdots \tag{3.17}$$

Then, substituting the above into the RTE,

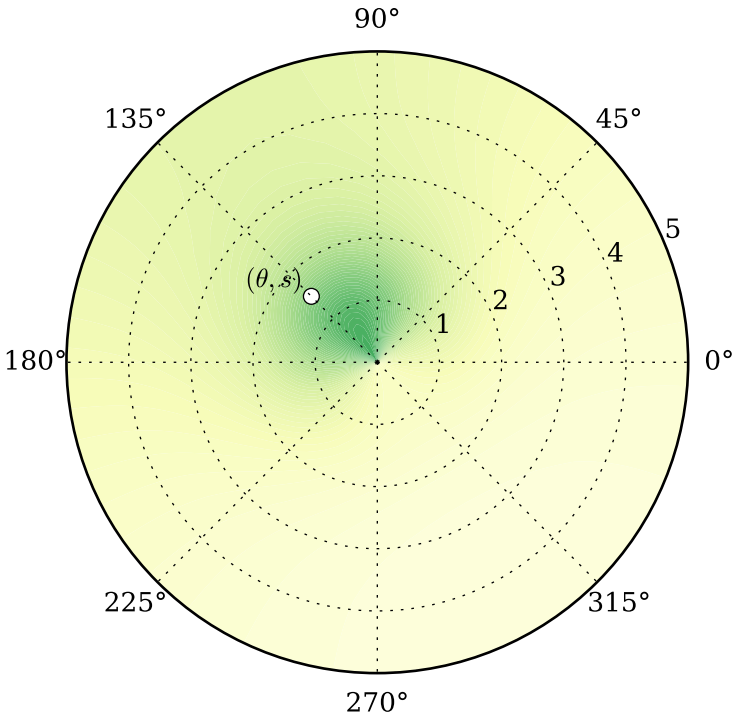

Figure 3.3: Contour plot of the probability of occupying sampled at 121 points using $\theta_f = 2\pi/3, v_w = 1$

$$
\begin{aligned}
&\vec{\omega} \cdot \nabla \left[L_0(\vec{x}, \vec{\omega}) + bL_1(\vec{x}, \vec{\omega}) + b^2 L_2(\vec{x}, \vec{\omega}) + \cdots \right] \\
&+ a(\vec{x}) \left[L_0(\vec{x}, \vec{\omega}) + bL_1(\vec{x}, \vec{\omega}) + b^2 L_2(\vec{x}, \vec{\omega}) + \cdots \right] \\
&= b \Bigg(\int_{4\pi} \beta(|\vec{\omega} - \vec{\omega}'|) \left[L_0(\vec{x}, \vec{\omega}') + bL_1(\vec{x}, \vec{\omega}') + b^2 L_2(\vec{x}, \vec{\omega}') + \cdots \right] d\vec{\omega}' \\
&- \left[L_0(\vec{x}, \vec{\omega}) + bL_1(\vec{x}, \vec{\omega}) + b^2 L_2(\vec{x}, \vec{\omega}) + \cdots \right] \Bigg)
\end{aligned}
\tag{3.18}
$$

Now, grouping like powers of b, we have the decopled set of equations

$$\vec{\omega} \cdot \nabla L_0(\vec{x}, \vec{\omega}) + a(\vec{x}) L_0(\vec{x}) = 0 \tag{3.19}$$

$$\vec{\omega} \cdot \nabla L_1(\vec{x}, \vec{\omega}) + a(\vec{x}) L_1(\vec{x}) = \int_{4\pi} \beta(|\vec{\omega} - \vec{\omega}'|) L_0(\vec{x}, \vec{\omega}')\, d\vec{\omega}' - L_0(\vec{x}, \vec{\omega}) \tag{3.20}$$

$$\vec{\omega} \cdot \nabla L_2(\vec{x}, \vec{\omega}) + a(\vec{x}) L_2(\vec{x}) = \int_{4\pi} \beta(|\vec{\omega} - \vec{\omega}'|) L_1(\vec{x}, \vec{\omega}')\, d\vec{\omega}' - L_1(\vec{x}, \vec{\omega}) \tag{3.21}$$

$$\vdots$$

3.2.2 Boundary Conditions

We use periodic boundary conditions in the x and y directions.

$$L\left((x_{\min}, y, z), \vec{\omega}\right) = L\left((x_{\max}, y, z), \vec{\omega}\right) \tag{3.22}$$

$$L\left((x, y_{\min}, z), \vec{\omega}\right) = L\left((x, y_{\max}, z), \vec{\omega}\right) \tag{3.23}$$

In the z direction, we specify a spatially uniform downwelling light just under the surface of the water by a function $f(\vec{\omega})$.

* $z_{\min}$ could also be much lower, e.g. 5m.

Further, we assume that no upwelling light enters the domain from the bottom.

$$L(\vec{x_s}, \vec{\omega}) = f(\omega) \text{ if } \vec{\omega} \cdot \hat{z} > 0 \tag{3.24}$$

$$L(\vec{x_b}, \vec{\omega}) = 0 \text{ if } \vec{\omega} \cdot \hat{z} < 0 \tag{3.25}$$

3.2.3 Rewrite as ODE along ray path

For all $\vec{x}, \vec{\omega}$, let

$$\tilde{a}(s) = a(\vec{l}(\vec{x}, \vec{\omega}), s), \tag{3.26}$$

$$\frac{du_0}{ds}(s) + \tilde{a}(s)u_0(s) = 0, u_0(0) = f(\vec{\omega}) \tag{3.27}$$

Then,

$$u_0(s) = f(\omega) \exp\left(-\int_0^s \tilde{a}(s)\, ds\right), \tag{3.28}$$

$$L_0(\vec{l}(\vec{x}, \vec{\omega}, s), \vec{\omega}) = u_0(s) \tag{3.29}$$

$$g_n(s) = \int_{4\pi} \beta(|\vec{\omega} - \vec{\omega}'|) L_{n-1}(\vec{l}(\vec{x}, \vec{\omega'}, s), \vec{\omega}')\, d\vec{\omega}' - L_{n-1}(\vec{l}(\vec{x}, \vec{\omega}, s), \vec{\omega}) \tag{3.30}$$

$$\frac{du_n}{ds}(s) + \tilde{a}(s)u_n(s) = g_n(s), u_n(0) = 0 \tag{3.31}$$

Then,

$$u_n(s) = \int_0^s g_n(s') \exp\left(-\int_{s''}^{s'} \tilde{a}(s'')\, ds''\right) ds' \tag{3.32}$$

$$L_n(\vec{l}(\vec{x}, \vec{\omega}, s), \vec{\omega}) = u_n(s) \tag{3.33}$$

CHAPTER IV

NUMERICAL IMPLEMENTATION

4.1 Kelp Numerics

4.1.1 Superindividuals

The kelp lifecycle model of which this work is part is based on the concept of superindividuals, which are kelp fronds which represent a subpopulation of identical fronds.

** WE HAVE TO CALCULATE LENGTH BEFORE CALCULATING STANDARD DISTRIBUTION **

At each depth k, we have n superindividuals, indexed by i. Superindividual i has a frond area a_{ki} and represents n_{ki} individual fronds.

4.1.2 Length Distribution

Given the superindividual data, we calculate the mean μ and standard deviation σ frond lengths using the formulas:

$$\mu_k = \frac{\sum_{i=1}^{N} a_{ki}}{\sum_{i=1}^{N} n_{ki}} \tag{4.1}$$

$$\sigma_k = \frac{\sum_{i=1}^{N} (a_{ki} - \mu_k)^2}{\sum_{i=1}^{N} n_{ki}} \tag{4.2}$$

We then assume that frond lengths are normally distributed in each depth layer with mean μ_k and standard deviation σ_k.

4.2 Discrete Grid

Following is a description of the uniform, rectangular spatial-angular grid used in the numerical implementation of this model. It is assumed that all simulated quantities are constant over the interior of a grid cell. The following indices are assigned to each dimension:

$$x \to i \tag{4.3}$$

$$y \to j \tag{4.4}$$

$$z \to k \tag{4.5}$$

$$\theta \to l \tag{4.6}$$

$$\phi \to m \tag{4.7}$$

Then, the center of a generic grid cell will be denoted as $(x_i, y_j, z_k, \theta_l, \phi_m)$, and the boundaries between adjacent grid cells will be referred to as *edges*. The number of grid points in each dimension are denoted by n_x, n_y, n_z, n_θ, and n_ϕ, with uniform spacings dx, dy, dz, $d\theta$, and $d\phi$ between adjacent grid points. Each

dimension has the same number of edges as cells. One-indexing will be employed throughout this document.

4.2.1 Spatial Grid

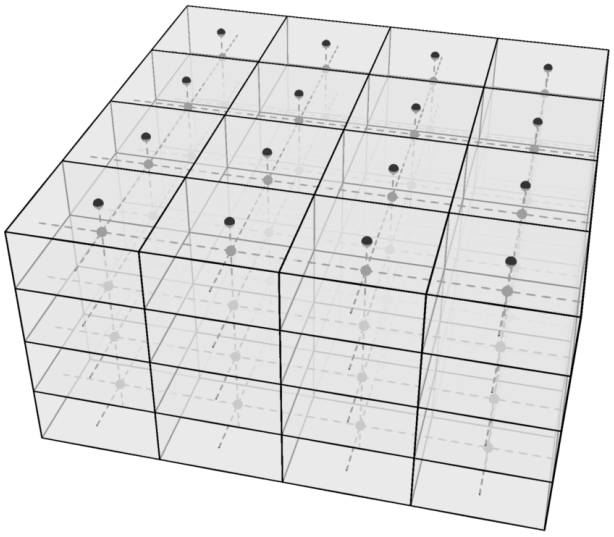

Figure 4.1: Spatial grid

$$dx = \frac{x_{\max} - x_{\min}}{n_x} \tag{4.8}$$

$$dy = \frac{y_{\max} - y_{\min}}{n_y} \tag{4.9}$$

$$dz = \frac{z_{\max} - z_{\min}}{n_z} \tag{4.10}$$

Then,

$$x_i = (i - 1/2)dx \tag{4.11}$$

$$y_j = (j - 1/2)dy \tag{4.12}$$

$$z_k = (k - 1/2)dz \tag{4.13}$$

4.2.2 Angular Grid

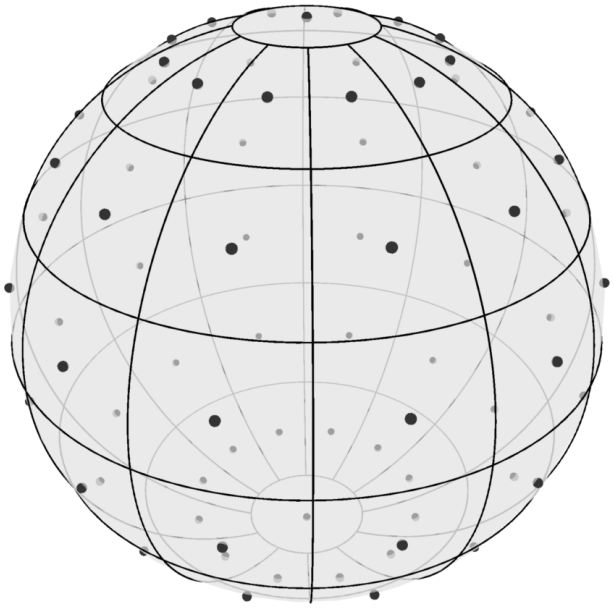

Figure 4.2: Angular grid

The azimuthal dimension is unique in that its extreme values are grid centers. That is,

$$\phi_1 = 0, \tag{4.14}$$

$$\phi_{n_\phi} = \pi. \tag{4.15}$$

Meanwhile, θ is similar to the spatial dimensions in that its extreme values are not grid centers. Then,

$$d\theta = \frac{2\pi}{n_\theta}, \tag{4.16}$$

$$d\phi = \frac{\pi}{n_\phi - 1}. \tag{4.17}$$

Then,

$$\theta_l = (l-1)d\theta, \tag{4.18}$$

$$\phi_m = (m-1)d\phi \tag{4.19}$$

It is also useful to define the edges between angular grid cells as

$$\theta_l^e = (l-1/2)d\theta, \qquad l = 1, \ldots, n_\theta \tag{4.20}$$

$$\phi_m^e = (m-1/2)d\phi, \quad m = 1, \ldots, n_\phi - 1. \tag{4.21}$$

As shown in Figure 4.2, $\phi = 0$ and $\phi = \pi$, called the north $(+z)$ and south $(-z)$ poles respectively, are treated separately. The total number of angles considered is $n_{\vec{\omega}} = n_\phi n_\theta - 2(n_\theta - 1)$. Since the poles create a non-rectangular angular grid in the sense that $n_{\vec{\omega}}$ is not the product of two integers, it is advantageous to use a single variable $p = 1, \ldots, n_{\vec{\omega}}$ to index angles $\vec{\omega} = (\theta, \phi)$ such that $p \in \{1, \ldots, n_{\vec{\omega}} - 2\}$ refers to the interior of the angular grid, and $p = (n_{\vec{\omega}} - 1)$ and $p = n_{\vec{\omega}}$ refer to the north and south poles respectively. The following notation is used.

$$\hat{l}(p) = \mod(p, n_\theta) + 1 \tag{4.22}$$

$$\hat{m}(p) = \text{ceil}(p/n_\theta) \tag{4.23}$$

$$\hat{\theta}_p = \theta_{\hat{l}(p)} \tag{4.24}$$

$$\hat{\phi}_p = \phi_{\hat{m}(p)} \tag{4.25}$$

Thus, it follows that

$$p = (\hat{m}(p) - 1)\, n_\theta + \hat{l}(p). \tag{4.26}$$

Accordingly, we define

$$\hat{p}(l,m) = (m-1)n_\theta + l. \tag{4.27}$$

4.2.3 Angular Quadrature

We assume that all quantities are constant within a spatial-angular grid cell. We therefore employ the midpoint rule for both spatial and angular integration.

** Need to define $\mathcal{X}$ in this context and write f explicitly as sum over grid cells.

** Is $d\theta$, etc. for both differential and grid spacing confusing?

$$\int_{4\pi} f(\vec{\omega})\, d\vec{\omega} = \int_0^{2\pi}\int_0^{\pi} f(\theta,\phi)\sin(\phi)\, d\phi\, d\theta \tag{4.28}$$

$$= \text{poles} + \int_0^{2\pi}\int_0^{\pi}\sum_{l=1}^{n_\theta}\sum_{m=2}^{n_\phi-1}\mathcal{X}_l(\theta)\mathcal{X}_m(\phi) f_{\hat{p}(l,m)}\sin(\phi)\, d\phi\, d\theta \tag{4.29}$$

$$= \text{poles} + \sum_{l=1}^{n_\theta}\sum_{m=2}^{n_\phi-1} f_{\hat{p}(l,m)}\int_{\theta_l^e}^{\theta_{l+1}^e}\int_{\phi_m^e}^{\phi_{m+1}^e}\sin(\phi)\, d\phi\, d\theta \tag{4.30}$$

$$= \text{poles} + d\theta\sum_{l=1}^{n_\theta}\sum_{m=2}^{n_\phi-1} f_{\hat{p}(l,m)}\int_{\phi_m^e}^{\phi_{m+1}^e}\sin(\phi)\, d\phi \tag{4.31}$$

$$= 2\pi\cos(\frac{d\phi}{2})\,(f_{n_{\vec{\omega}}-1} + f_{\vec{\omega}}) \tag{4.32}$$

$$+ d\theta\sum_{l=1}^{n\theta}\sum_{m=1}^{n\phi} f_{\hat{p}(l,m)}\left(\cos(\phi_m^e) - \cos(\phi_{m+1}^e)\right)$$

Let

$$\delta_p = \cos(\phi^e_{\hat{m}(p)}) - \cos(\phi^e_{\hat{m}(p)+1}). \tag{4.33}$$

Then,

$$\int_{4\pi} f(\vec{\omega})\, d\vec{\omega} = 2\pi \cos(\frac{d\phi}{2})\,(f_{n_{\vec{\omega}}-1} + f_{\vec{\omega}}) + d\theta \sum_{p=1}^{n_{\vec{\omega}}-2} f_p \delta_p \tag{4.34}$$

urface Note that 0 is not stored as a grid center in any spatial dimension. Radiance values for the surface boundary condition are stored separately as the array (f_p).

4.2.4 Discrete Variable Notation

L_{ijkp}, a_{ijk}, f_p

4.3 Finite Difference

4.3.1 Discretization

For the spatial interior of the domain, we use the 2nd order central difference formula (CD2) to approximate the derivatives, which is

$$f'(x) = \frac{f(x+dx) - f(x-dx)}{2dx} + \mathcal{O}(dx^3). \tag{CD2}$$

When applying the PDE on the upper or lower boundary, we use the forward and backward difference (FD2 and BD2) formulas respectively. Omitting $\mathcal{O}(dx^3)$, we have

$$f'(x) = \frac{-3f(x) + 2f(x+dx) - f(x+2dx)}{2dx} \tag{FD2}$$

$$f'(x) = \frac{3f(x) - 2f(x-dx) + f(x-2dx)}{2dx} \tag{BD2}$$

For the upper and lower boundaries, we need an asymmetric finite difference method. In general, the Taylor Series of a function f about x is

$$f'(x+\varepsilon) = \sum_{n=1}^{\infty} \frac{f^{(n)}(x)}{n!}\varepsilon^n \tag{4.35}$$

Truncating after the first few terms, we have

$$f'(x+\varepsilon) = f(x) + f'(x)\varepsilon + \frac{f''(x)}{2}\varepsilon^2 + \mathcal{O}(\varepsilon^3) \tag{4.36}$$

Similarly, replacing ε with $-\varepsilon/2$ we have

$$f'(x-\frac{\varepsilon}{2}) = f(x) - \frac{f'(x)\varepsilon}{2} + \frac{f''(x)\varepsilon^2}{8} + \mathcal{O}(\varepsilon^3). \tag{4.37}$$

Rearranging (4.36) produces

$$f''(x)\varepsilon^2 = 2f(x+\varepsilon) - 2f(x) - 2f'(x)\varepsilon + \mathcal{O}(\varepsilon^3) \tag{4.38}$$

Combining (4.37) with (4.38) gives

$$\begin{aligned}
\varepsilon f'(x) &= 2f(x) - 2f(x-\frac{\varepsilon}{2}) + f''(x)\frac{\varepsilon^2}{8} + \mathcal{O}(\varepsilon^3) \\
&= 2f(x) - 2f(x-\frac{\varepsilon}{2}) + \frac{f(x+\varepsilon)}{4} - \frac{f(x)}{4} - \frac{f'(x)\varepsilon}{4} + \mathcal{O}(\varepsilon^3) \\
&= \frac{4}{5}\left(2f(x) - 2f(x-\frac{\varepsilon}{2}) + \frac{f(x+\varepsilon)}{4} - \frac{f(x)}{4}\right) + \mathcal{O}(\varepsilon^3)
\end{aligned}$$

Then, dividing by ε gives

$$f'(x) = \frac{-8f(x-\frac{\varepsilon}{2}) + 7f(x) + f(x+\varepsilon)}{5\varepsilon} + \mathcal{O}(\varepsilon^2) \tag{4.39}$$

Similarly, substituting $\varepsilon \to -\varepsilon$, we have

$$f'(x) = \frac{-f(x-\varepsilon) - 7f(x) + 8f(x+\frac{\varepsilon}{2})}{5\varepsilon} + \mathcal{O}(\varepsilon^2) \tag{4.40}$$

4.3.2 Difference Equation

* Periodic x, y

Interior:

$$\begin{aligned}
&\frac{L_{i+1,jkp} - L_{i-1,jkp}}{2dx} \sin\hat{\phi}_p \cos\hat{\theta}_p \\
&+\frac{L_{i,j+1,kp} - L_{i,j-1,kp}}{2dy} \sin\hat{\phi}_p \sin\hat{\theta}_p \\
&+\frac{L_{ij,k+1,p} - L_{ij,k-1,p}}{2dz} \cos\hat{\phi}_p + (a_{ijk} + b) L_{ijkp} \\
&-2\pi \cos\left(\frac{d\theta}{2}\right) (L_{ijk,n_{\vec{\omega}}-1} + L_{ijk,n_{\vec{\omega}}}) \\
&-d\theta \sum_{\substack{p'=1 \\ p' \neq p}}^{n_{\vec{\omega}}-2} L_{ijkp'} \delta_{p'} = 0
\end{aligned} \tag{4.41}$$

Note that when discretizing the integral, we exclude the $p' = p$ term of the sum. This is because that term corresponds to "scattering" straight ahead ($|\vec{\omega} - \vec{\omega}'| = 0$), which is in fact not scattering at all, but rather transmission.

Surface downwelling (BC):

$$\begin{aligned}
&\frac{L_{i+1,jkp} - L_{i-1,jkp}}{2dx} \sin\hat{\phi}_p \cos\hat{\theta}_p \\
&+\frac{L_{i,j+1,kp} - L_{i,j-1,kp}}{2dy} \sin\hat{\phi}_p \sin\hat{\theta}_p \\
&+\frac{-8f_p + 7L_{ijkp} + L_{ij,k+1,p}}{5dz} \cos\hat{\phi}_p + (a_{ijk} + b) L_{ijkp} \\
&-2\pi \cos\left(\frac{d\theta}{2}\right) (L_{ijk,n_{\vec{\omega}}-1} + L_{ijk,n_{\vec{\omega}}}) \\
&-d\theta \sum_{\substack{p'=1 \\ p' \neq p}}^{n_{\vec{\omega}}-2} L_{ijkp'} \delta_{p'} = 0
\end{aligned}$$

Combining L_{ijkp} terms on the left and moving the boundary condition to the right gives

$$
\begin{aligned}
&\frac{L_{i+1,jkp} - L_{i-1,jkp}}{2dx} \sin\hat{\phi}_p \cos\hat{\theta}_p \\
&+\frac{L_{i,j+1,kp} - L_{i,j-1,kp}}{2dy} \sin\hat{\phi}_p \sin\hat{\theta}_p \\
&+\frac{L_{ij,k+1,p}}{5dz} \cos\hat{\phi}_p + (a_{ijk} + b + \frac{7}{5dz}) L_{ijkp} \\
&-2\pi \cos\left(\frac{d\theta}{2}\right) (L_{ijk,n_{\vec{\omega}}-1} + L_{ijk,n_{\vec{\omega}}}) \\
&-d\theta \sum_{\substack{p'=1 \\ p' \neq p}}^{n_{\vec{\omega}}-2} L_{ijkp'} \delta_{p'} = \frac{8 f_p}{5dz}.
\end{aligned}
\tag{4.42}
$$

Likewise for the bottom boundary condition, we have

$$
\begin{aligned}
&\frac{L_{i+1,jkp} - L_{i-1,jkp}}{2dx} \sin\hat{\phi}_p \cos\hat{\theta}_p \\
&+\frac{L_{i,j+1,kp} - L_{i,j-1,kp}}{2dy} \sin\hat{\phi}_p \sin\hat{\theta}_p \\
&-\frac{L_{ij,k-1,p}}{5dz} \cos\hat{\phi}_p + (a_{ijk} + b - \frac{7}{5dz}) L_{ijkp} \\
&-2\pi \cos\left(\frac{d\theta}{2}\right) (L_{ijk,n_{\vec{\omega}}-1} + L_{ijk,n_{\vec{\omega}}}) \\
&-d\theta \sum_{\substack{p'=1 \\ p' \neq p}}^{n_{\vec{\omega}}-2} L_{ijkp'} \delta_{p'} = 0.
\end{aligned}
\tag{4.43}
$$

Now, for upwelling light at the first depth layer (non-BC), we apply FD2.

$$
\begin{aligned}
&\frac{L_{i+1,jkp} - L_{i-1,jkp}}{2dx} \sin\hat{\phi}_p \cos\hat{\theta}_p \\
&+\frac{L_{i,j+1,kp} - L_{i,j-1,kp}}{2dy} \sin\hat{\phi}_p \sin\hat{\theta}_p \\
&+\frac{-3L_{ijkp} + 2L_{ij,k+1,p} - L_{ij,k+2,p}}{2dz} \cos\hat{\phi}_p + (a_{ijk} + b) L_{ijkp} \\
&-2\pi \cos\left(\frac{d\theta}{2}\right) (L_{ijk,n_{\vec{\omega}}-1} + L_{ijk,n_{\vec{\omega}}}) \\
&-d\theta \sum_{\substack{p'=1 \\ p' \neq p}}^{n_{\vec{\omega}}-2} L_{ijkp'} \delta_{p'} = 0
\end{aligned}
\tag{4.44}
$$

Grouping L_{ijkp} terms gives

$$\begin{aligned}
&\frac{L_{i+1,jkp} - L_{i-1,jkp}}{2dx} \sin\hat{\phi}_p \cos\hat{\theta}_p \\
&+\frac{L_{i,j+1,kp} - L_{i,j-1,kp}}{2dy} \sin\hat{\phi}_p \sin\hat{\theta}_p \\
&+\frac{2L_{ij,k+1,p} - L_{ij,k+2,p}}{2dz} \cos\hat{\phi}_p + \left(a_{ijk} + b - 3\frac{\cos\hat{\phi}_p}{2dz}\right) L_{ijkp} \\
&-2\pi \cos\left(\frac{d\theta}{2}\right) \left(L_{ijk,n_{\vec{\omega}}-1} + L_{ijk,n_{\vec{\omega}}}\right) \\
&-d\theta \sum_{\substack{p'=1 \\ p'\neq p}}^{n_{\vec{\omega}}-2} L_{ijkp'}\delta_{p'} = 0
\end{aligned} \tag{4.45}$$

Similarly, for downwelling light at the lowest depth layer, we have

$$\begin{aligned}
&\frac{L_{i+1,jkp} - L_{i-1,jkp}}{2dx} \sin\hat{\phi}_p \cos\hat{\theta}_p \\
&+\frac{L_{i,j+1,kp} - L_{i,j-1,kp}}{2dy} \sin\hat{\phi}_p \sin\hat{\theta}_p \\
&+\frac{-2L_{ij,k-1,p} + L_{ij,k-2,p}}{2dz} \cos\hat{\phi}_p + \left(a_{ijk} + b + 3\frac{\cos\hat{\phi}_p}{2dz}\right) L_{ijkp} \\
&-2\pi \cos\left(\frac{d\theta}{2}\right) \left(L_{ijk,n_{\vec{\omega}}-1} + L_{ijk,n_{\vec{\omega}}}\right) \\
&-d\theta \sum_{\substack{p'=1 \\ p'\neq p}}^{n_{\vec{\omega}}-2} L_{ijkp'}\delta_{p'} = 0
\end{aligned} \tag{4.46}$$

4.3.3 Structure of Linear System

Describe layout of matrix.

Number of rows/columns: $n_x n_y n_z n_{\vec{\omega}}$

Number of nonzero RHS entries: $n_x n_y n_z$

** Table with number of nonzero matrix entries in each type of row (interior, exterior-BC, exterior non-BC)

Number of nonzero matrix entries: $n_x n_y n_{\vec{\omega}} \left[n_z(n_{\vec{\omega}} + 6) - 1\right]$

4.4 GMRES

GMRES is a Krylov Subspace method. These work like this. Here's what's special about GMRES. Advantages. Drawbacks. Not practical for running in SINMOD.

4.5 Numerical Asymptotics

4.5.1 Ray Tracing Algorithm

Extract values along path

In order to evaluate a path integral through the previously described grid, it is first necessary to construct a one-dimensional piecewise constant integrand which is discontinuous at unevenly spaced points corresponding to the intersections between the path and edges in the spatial grid.

Consider a grid center $\vec{x_1} = (x_1, y_1, z_1)$ and a corresponding path $\vec{l}(\vec{x_1}, \vec{\omega}, s)$. To find the location of discontinuities in the itegrand, we first calculate the distance from its origin, $\vec{x_0}(\vec{x_1}, \vec{\omega}) = (x_0, y_0, z_0)$ to grid edges in each dimension separately.

** THIS NOTATION IS OVERLOADED **

Given

$$x_i = x_0 + s_i^x/\tilde{s}(x_1 - x_0) \tag{4.47}$$

$$y_j = y_0 + s_j^y/\tilde{s}(y_1 - y_0) \tag{4.48}$$

$$z_k = z_0 + s_k^z/\tilde{s}(z_1 - z_0) \tag{4.49}$$

we have

$$s_i^x = \tilde{s}\frac{x_i - x_0}{x_1 - x_0} \tag{4.50}$$

$$s_i^y = \tilde{s}\frac{y_i - y_0}{y_1 - y_0} \tag{4.51}$$

$$s_i^z = \tilde{s}\frac{z_i - z_0}{z_1 - z_0} \tag{4.52}$$

$$\tag{4.53}$$

Then, move to the adjacent grid cell in the dimension which requires the shortes step to reach an edge. Save ds of the path through this cell. Also save abs. coef. and source. ** Definitely needs more work**

- absorption coefficient ($\tilde{a}(s)$)

- effective source ($g_n(s)$)

Ray integral

Here are the equations for calculating the double integral over ray paths required for the asymptotics. It will hopefully make more sense once I add words to accompany the symbols.

Let

$$g_n(s) = \sum_{i=1}^{N-1} g_{ni}\mathcal{X}_i(s) \tag{4.54}$$

$$\tilde{a}(s) = \sum_{i=1}^{N-1} \tilde{a}_i\mathcal{X}_i(s) \tag{4.55}$$

$$\tag{4.56}$$

and

$$\mathcal{X}_i(s) = \begin{cases} 1, & a_I \leq s < s_{i+1} \\ \\ 0, & \text{otherwise} \end{cases} \tag{4.57}$$

and $\{s_i\}_{i=1}^N$ is increasing.

Let $ds_i = s_{i+1} - s_i$.

Let $\hat{i}(s) = \min\{i \in \{1, \ldots, N\} : s_i > s\}$. Let $\tilde{d}(s) = s_{\hat{i}(s)} - s$.

We have $s_1 = 0$ and $s_N = \tilde{s}$.

$$u_n(\tilde{s}) = \int_0^{\tilde{s}} g_n(s') \exp\left(-\int_{s''}^{s'} \tilde{a}(s'')\, ds''\right) ds' \tag{4.58}$$

$$= \int_0^{s_N} \sum_{i=1}^{N-1} g_{ni} \mathcal{X}_i(s') \exp\left(-\int_{s''}^{s'} \sum_{j=1}^{N-1} \tilde{a}_j \mathcal{X}_j(s'')\, ds''\right) ds' \tag{4.59}$$

$$= \sum_{i=1}^{N-1} g_{ni} \int_0^{s_N} \mathcal{X}_i(s') \exp\left(-\sum_{j=1}^{N-1} \tilde{a}_j \int_{s''}^{s'} \mathcal{X}_j(s'')\, ds''\right) ds' \tag{4.60}$$

$$= \sum_{i=1}^{N-1} g_{ni} \int_{s_i}^{s_{i+1}} \exp\left(-\tilde{a}_{\hat{i}(s')-1} \tilde{d}(s') - \sum_{j=\hat{i}(s')}^{N-1} \tilde{a}_j ds_j\right) ds' \tag{4.61}$$

$$= \sum_{i=1}^{N-1} g_{ni} \int_{s_i}^{s_{i+1}} \exp\left(-\tilde{a}_i (s_{i+1} - s') - \sum_{j=i+1}^{N-1} \tilde{a}_j ds_j\right) ds' \tag{4.62}$$

Let

$$b_i = -\tilde{a}_i s_{i+1} - \sum_{j=i+1}^{N-1} \tilde{a}_j ds_j. \tag{4.63}$$

Then,

$$u_n(\tilde{s}) = \sum_{i=1}^{N-1} g_{ni} \int_{s_i}^{s_{i+1}} \exp\left(\tilde{a}_i s' + b_i\right) ds' \tag{4.64}$$

Let

$$d_i = \int_{s_i}^{s_{i+1}} \exp\left(\tilde{a}_i s' + b_i\right)\, ds' \tag{4.65}$$

$$= \begin{cases} ds_i \exp(b_i), & \tilde{a} = 0 \\ \left(\exp(\tilde{a}_i s_{i+1}) - \exp(\tilde{a}_i s_i)\right)/\tilde{a}_i, & \text{otherwise} \end{cases} \tag{4.66}$$

Then,

$$u_n(\tilde{s}) = \sum_{i=1}^{N-1} g_{ni} d_i \tag{4.67}$$

CHAPTER V

NUMERICAL ANALYSIS

5.1 Grid Study

Run many grid sizes with GMRES, using asymptotic solution as initial guess. Compare CPU times and accuracy, assuming largest grid is "true" solution. Determine necessary grid size to achieve reasonable accuracy.

5.2 Asymptotics vs. Finite Difference

Compare asymptotic solutions to GMRES with reasonable grid size as determined above. Compare CPU time and accuracy. Determine ideal number of scatters to include (number of terms in asymptotic series). Repeat for a few values of scattering coefficient.

5.3 Parameter Study

Vary parameters and measure average differences in radiance for full grid, as well as average irradance over depth.

- absorption coefficient
- scattering coefficient

- VSF

- frond bending coefficient

CHAPTER VI

EXPERIMENTAL DETERMINATION OF PARAMETERS

It looks like we probably won't be able to get the synthetic kelp to actually do the experiments, but I'll describe what one would do in order to determine "frond bending coefficients", as well as optical properties of water and kelp, citing literature and reporting values obtained by others.

6.1 Optical Properties

6.1.1 Absorption Coefficients

subsectionScattering Coefficients

6.1.2 Volume Scattering Function

6.2 Frond Distribution Parameters

6.2.1 Rotation

6.2.2 Lift

CHAPTER VII

SIMULATION RESULTS

Run Ole Jacob's model with my new light model, compare:

- irrad over time for several depths
- computation time
- harvestable biomass

CHAPTER VIII

CONCLUSION

It was great and I've survived so far. Does future work go here?

BIBLIOGRAPHY

[1] Nick Anderson. A mathematical model for the growth of giant kelp. *Simulation*, 22(4):97–105, 1974.

[2] G. A. Jackson. Modelling the growth and harvest yield of the giant kelp Macrocystis pyrifera. *Marine Biology*, 95(4):611–624, 1987.

[3] M. A. Burgman and V. A. Gerard. A stage-structured, stochastic population model for the giant kelpMacrocystis pyrifera. *Marine Biology*, 105(1):15–23, 1990.

[4] Melvin Nyman, Murray Brown, Michael Neushul, and Jonathan A. Keogh. *Macrocystis pyrifera in New Zealand: testing two mathematical models for whole plant growth*, volume 2. September 1990. DOI: 10.1007/BF02179782.

[5] Pedro Duarte and J. G. Ferreira. A model for the simulation of macroalgal population dynamics and productivity. *Ecological modelling*, 98(2-3):199–214, 1997.

[6] Akira Yoshimori, Tokihiro Kono, and Hitoshi Iizumi. Mathematical models of population dynamics of the kelp Laminaria religiosa, with emphasis on temperature dependence. *Fisheries Oceanography*, 7(2):136146, 1998.

[7] Ole Jacob Broch and Dag Slagstad. Modelling seasonal growth and composition of the kelp Saccharina latissima. *Journal of Applied Phycology*, 24(4):759–776, August 2012.

[8] Paul Wassmann, Dag Slagstad, Christian Wexels Riser, and Marit Reigstad. Modelling the ecosystem dynamics of the Barents Sea including the marginal ice zone. *Journal of Marine Systems*, 59(1-2):1–24, January 2006.

[9] C.D. Mobley. Radiative Transfer in the Ocean. In *Encyclopedia of Ocean Sciences*, pages 2321–2330. Elsevier, 2001. DOI: 10.1006/rwos.2001.0469.